IEEE Access
Multidisciplinary | Rapid Review | Open Access Journal

Received May 2, 2019, accepted May 16, 2019, date of publication May 24, 2019, date of current version June 10, 2019.

Digital Object Identifier 10.1109/ACCESS.2019.2918953

A Review on Variable Flux Machine Technology: Topologies, Control Strategies and Magnetic Materials

REKHA JAYARAJAN, (Student Member, IEEE), NUWANTHA FERNANDO, (Member, IEEE), AND INAM ULLAH NUTKANI, (Senior Member, IEEE)
School of Engineering, RMIT University, Melbourne, VIC 3000, Australia

Corresponding author: Nuwantha Fernando (nfdo@ieee.org)

This work was supported by RMIT University and the Australian Government Research Training Program (RTP) Scholarship.

ABSTRACT Modern applications demand challenging operation requirements from electrical machines. Variable-flux machine (VFM) concepts are found to offer new opportunities for improved machine design. This paper reviews the VFM technology. Three topologies, mainly the parallel hybrid VFMs, series hybrid VFMs, and variable-flux flux intensifying type VFMs are discussed in detail. The variable-flux flux Intensifying machines are found to be the state-of-the-art VFM technology available to-date. The paper also reviews the magnetization process in the VFMs and relates this with the B-H curve of the magnetic material. The conventional PM machine mathematical model is adapted to represent the operation of the VFMs. The different operational limitations of the VFMs are explained and the different modes of operation of the VFMs have been reviewed and compared. The magnetization state manipulation techniques are reviewed. The AC magnetization is found to be the more preferable approach to reduce weight and manufacturing complexity of the VFMs. The trapezoidal current pulse based approach is popular in AC magnetization state manipulation, however, new advanced forms of current vector trajectory control techniques offer comparatively better magnetic state manipulation and higher speed capability for remagnetization of the magnets in the VFMs. The paper also reviews the different magnetization state estimation techniques that are useful during control systems development for the VFMs. The magnetic material for the VFM design is reviewed and potential alternative magnetic material that can satisfy the requirements of the VFMs have been identified. Finally, the current status, challenges, and the potential of VFMs technology are discussed in the conclusion of the paper.

INDEX TERMS Variable flux machines, wide speed range, permanent magnet machines, field weakening, magnetic material, magnetization, demagnetization, machine design.

I. INTRODUCTION

Permanent Magnet (PM) machines are increasingly used in industrial applications that include power generation, transportation, and manufacturing. Recent technological advancements in electric vehicles, railway traction, ship propulsion, and electromobility are few key areas of application that have adopted PM machines technology in recent years. Due to the availability of a fixed magnetic field, PM machines can be designed for high torque and power density, high efficiency and lower heat production in the rotor compared with other types of electrical machines. However, further improvement opportunities exist with PM machine design. Two of the primary research questions associated with the manufacture and application of PM machines are:

Q1. Can PM machines be designed to achieve a wide torque-speed envelope with minimized energy losses caused by Field Weakening (FW)?

Q2. Can PM machines be designed with reduced rare earth material content?

In order to operate a PM machine in an extended speed range, it is necessary to weaken the magnetic field [1]–[3] as shown in Fig. 1. The negative direct axis opposing field is used to depress the PM field and thereby reduce the effective electromotive force (EMF) at high speeds. However, field weakening increases conduction losses as shown in Fig. 2 and increases the risk of irreversible demagnetization of the PMs during operation. Due to these concerns, current research in PM machine design attempts to answer question Q1 above.

The associate editor coordinating the review of this manuscript and approving it for publication was Ton Do.

TABLE 1. Nomenclature.

PM	Permanent Magnet
PMSM	Permanent Magnet Synchronous Machine
PMA-SynRM	Permanent Magnet Assisted Synchronous Reluctance
IPMSM	Interior Permanent Magnet Synchronous Machine
VFI-IPM	Variable-Flux Flux Intensifying IPM
VFM	Variable Flux Motor
MM	Memory Motor
VFMM	Variable Flux Memory Motors
VPM	Variable Permanent Magnet
CPM	Constant Permanent Magnet
REM	Rare Earth Magnet
PC	Permeance Coefficient
HCF	High Coercive Force
LCF	Low Coercive Force
MS	Magnetization State
CV	Current Vector
EVs	Electric Vehicles
FW	Flux Weakening
HEVs	Hybrid Electric Vehicles
HFI	High Frequency Injection
CPSR	Constant Power Speed Range
RRCVT	Reverse rotating current vector trajectory
SLλ^sT	Straight Line stationary frame flux linkage Trajectory

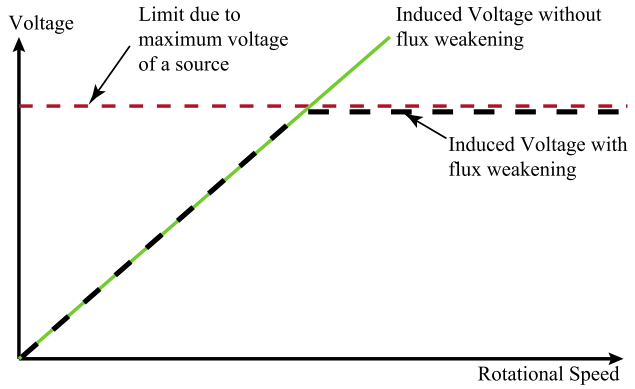

FIGURE 1. Magnetization as a function of applied field. It is good practice to explain the significance of the figure in the caption.

In addition to the above, the use of PM material with rare-earth compounds has also lead to economic issues with the manufacture of PM machines. The issues with the use of rare-earth PMs can be summarized as [4]:

1) The high cost and limited supply of rare-earth materials
2) Price oscillation of PM material due to political restrictions
3) The high environmental impact of mining, refining, and recycling of rare-earth compounds

Due to these concerns, current research in PM machine design also attempts the resolution of question Q2. Recent research in PM machines design has key developments in Variable Flux Machines (VFM) technology which can potentially change the speed range with minimal losses and also reduce the use of rare-earth magnets thereby answering both the above research questions.

This paper reviews the present state-of-the-art VFM development, control strategies, and materials. This paper is organized as follows: The VFM concept is presented in Section I and Section II focuses on the main VFM topologies. Section III reviews the magnetic characteristics and magnetization/demagnetization analysis of various magnets relevant to VFM design. VFM principle of operation is discussed in Section IV. Section V presents the Magnetization State manipulation techniques. The Magnetization State estimation principle and methods proposed to-date are discussed in Section VI. Section VII presents the developments in PM material technology that are relevant for VFM design. Section VIII concludes this review paper and identifies the future direction of VFM technology.

A. WHY VARIABLE FLUX MACHINES?

New techniques have been developed in recent years enabling the adjustment of air-gap flux in order to extend the speed/torque range of PM machines. VFMs for wide-speed operation was first proposed by Ostovic [7], [8]. VFMs can dynamically change the intensity of magnetization and memorize the flux density level in the rotor magnets, and therefore a class of VFMs is also referred to as Memory Motors [7].

State-of-the-art Electric Vehicles (EVs) and Hybrid Electric Vehicles (HEVs) use Interior Permanent Magnet Synchronous Motors (IPMSMs) to power the vehicle drivetrain. One of the main issues in the application of conventional PM machines is the potential mismatch between the region of high efficiency of the machine and region of highest operation duty of EVs/HEVs. VFMs with their wide and variable torque-speed envelope is a promising solution that could enable optimal operation under dynamically changing load conditions.

The high Curie temperature of LCF magnets allows VFMs to be used in harsh environments. Therefore VFMs could be a potential choice as generators in the microturbine embedded power generation applications where extended speed ranges, as well as high operating temperature (approx. 800°C), are the major challenges. VFMs have also been developed for laundry machines that require operation in dual modes, i.e., washing and dewatering [9]. The washing cycle requires low speed, and high torque, whereas the dewatering operation requires high-speed and low-torque.

The limited supply or uneconomical prices of Rare-Earth Magnets (REMs) is another driving force to find improved motor technologies that do not depend on REMs [10]. Low Coercive Force (LCF) magnet materials such as AlNiCo exhibit remanent flux densities close to REMs and are a potential replacement for REMs. However, LCF magnets are not widely used for PM machine design due to demagnetization phenomena that occur due to the armature field reaction. If a Permanent Magnet Synchronous Motor (PMSM) is designed with LCF magnets in such a way that the demagnetization effects are controllable, it will theoretically provide efficiencies and torque densities comparable to rare-earth PMSMs as both REMs and LCF magnets can provide comparable excitation fields.

VFMs use the inherent demagnetization property of LCFs to improve machine efficiency in the flux weakening region.

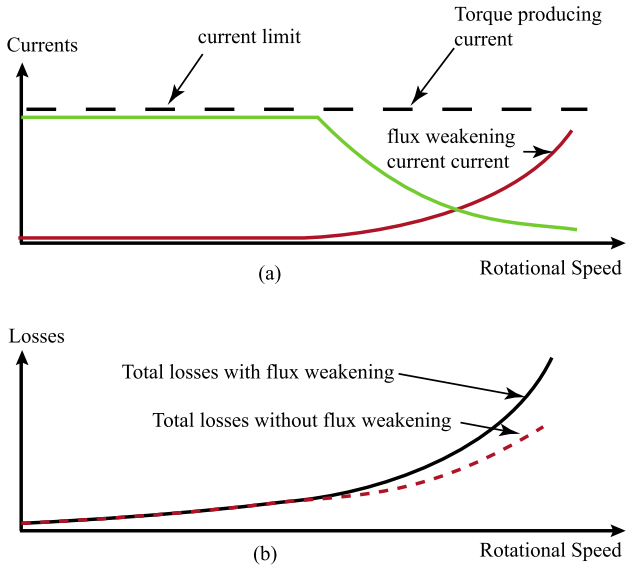

FIGURE 2. (a) Currents and (b) Losses of a PM motor operating from low to high speed.

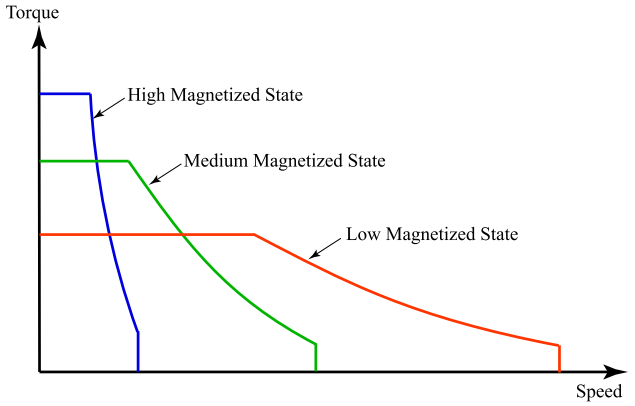

FIGURE 3. Extending the torque-speed range using Magnetization State manipulation.

As magnet flux can be reduced by the application of a demagnetizing current pulse, additional copper losses due to a continuous-time field weakening current as shown in Fig. 2 can be eliminated. The principle used to increase the torque-speed envelope for VFMs is shown in Fig. 3. The three profiles Fig. 3 indicate the torque-speed envelopes after the PMs are magnetized to three different magnetization states. The torque speed range can be extended as the magnetization levels are reduced, however, at the cost of reduced peak torque. Hence, in order to extend the torque-speed range and achieve high peak torque, the PMs need to be magnetized to high magnetization states at low speeds and as the speed increases, the magnetization of the PMs should be reduced accordingly. Recent research [11]–[17] techniques developed to achieve these features are reviewed in the following sections.

II. VARIABLE FLUX PM MACHINE TOPOLOGIES

The earliest form of VFMs are also referred to as Variable Flux Memory Motors (VFMMs). The motivation of VFMMs is to combine the high torque density of conventional PM flux machines [5], [18] with variable PM flux characteristics. The operating principle and the magnetization of the Memory Motor [6], [19]–[22] require the magnetic material to have low coercive force (LCF) and high remanent magnetic flux density. The low coercive force eases the demagnetization process whereas the high remanent magnetic flux density enhances the air gap flux and hence gives an improved machine torque. The first proposed VFMM was a PM motor with a single LCF magnet material as shown in Fig. 4 (a).

In this type of machine, the PMs are tangentially magnetized. The PMs can also be partially demagnetized by applying a reverse magnetizing field on the direct axis. The air-gap field can be varied in a fraction of synchronous stator current cycle period. VFMMs are typically designed such that the torque producing current component on the quadrature axis cannot demagnetize the PMs since the quadrature axis flux path is between the PM poles. Since the continuous field weakening current is not required, VFMMs, therefore, have a clear advantage over traditional PMSMs in-terms of lower copper losses.

Research on VFM design study PM positioning, number and shape of PMs and amount of magnet material as a means to improve performance. Takbash and Pillay [23], Hengchuan *et al.* [24] indicate that the PM shape has to be designed carefully to guarantee the demagnetization effects at flux weakening mode and to be able to remagnetize and maximize the utilization of the PMs. Spoke type rotor is also found to boost the utilization of PMs [25], [26]. However, these VFPM machines sacrifice torque density due to the use of weak Variable Permanent Magnets (VPMs) resulting in a reduction in air gap flux. An alternate approach is to have controllable PMs on the stator [27], [28]. These type of machines require an additional winding in the stator to control demagnetization and remagnetization process of the magnets. The torque density is compromised due to space taken up by the extra winding.

To improve the torque density of VFM machines, the concept of hybridization of the rotor with different magnet types is found to enhance the characteristics of memory motors with promising results [6], [29]–[34].

A. HYBRID MEMORY MOTORS:

Figures 4 (b) and 4(c) show two examples of hybrid memory motors. These type of VFMs use a Constant Permanent Magnet (CPM) made of High Coercive Force (HCF) material which provides a relatively constant field and the VPM made of LCF material which provides a variable flux component.

The structure of hybrid memory motors found in the literature are based on conventional IPMSMs, however with a modified rotor design as shown in Fig. 4 (b) and 4(c). Neodymium Iron Boron (NdFeB) magnets are usually adopted as the HCF magnets due to their high remanence and high coercive force, and Alnico(AlNiCo) magnets are generally used as the LCF magnets due to their high remanence and low coercive force. The demagnetization curves

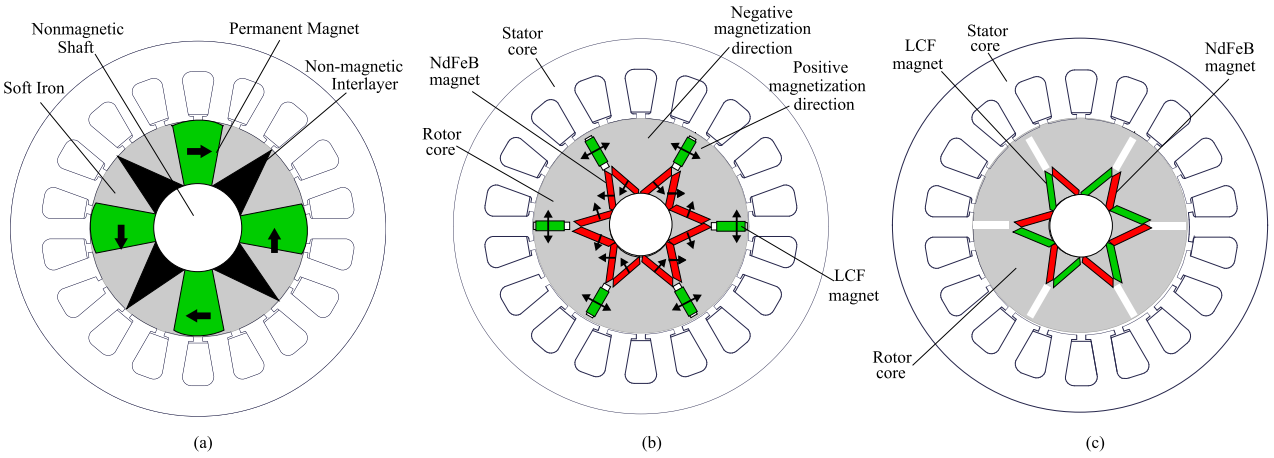

FIGURE 4. (a) Example cross section of a VFM with single PM material [5], (b) Parallel hybrid PM VFM [6] and (c) Series hybrid PM VFM.

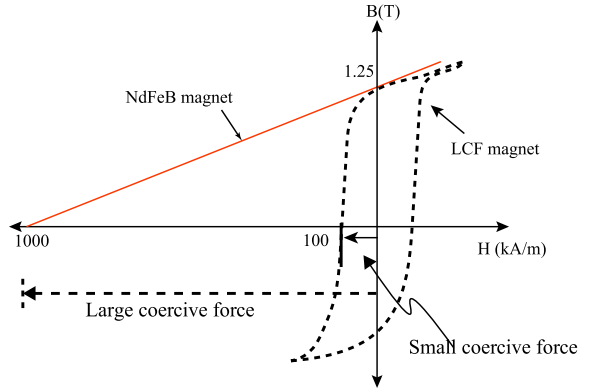

FIGURE 5. Magnetic characteristics of PM for variable flux motor.

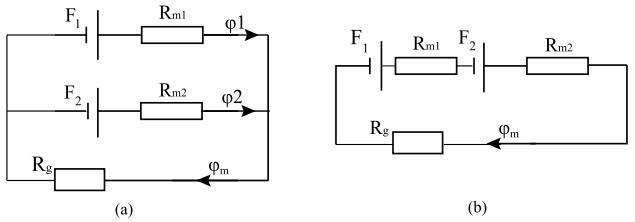

FIGURE 6. Equivalent magnetic circuits of hybrid VFM: (a) Parallel hybrid VFM and (b) Series hybrid VFM.

of example LCF and HCF magnets are shown in Fig. 5 and the comparative difference in the coercive force H_{ci} is highlighted.

The two types of PMs can be magnetically connected either in parallel or in series. Figure 4 (b) shows the parallel type and Fig. 4 (c) shows the series type VFM motors respectively. The lumped parameter equivalent magnetic circuit representation of these two types are shown in Fig. 6 (a) and (b) respectively. The parameters F_1, R_{m1} and F_2, R_{m2} represent the intrinsic Magnetomotive Force (MMF) and reluctance of CPMs and VPMs respectively. R_g is the equivalent air-gap reluctance. Magnetization/Demagnetization behaviour of parallel and series hybrid motor variants is reviewed below.

1) PARALLEL HYBRID MEMORY MOTORS

In the parallel circuit, the main flux through the air gap is the sum of two parallel branches i.e., the sum of CPM flux and VPM flux as shown in Fig. 6 (a). Research presented in [29] and [30] investigate this type of parallel magnet arrangement. VPM flux may be negative if MMF of the VPM F_2 is too low, which implies that CPM flux potentially short circuits via VPM branch, and it may even demagnetize the VPM if the two branches are not balanced. The authors of [31] observed that cross-coupling between the two magnets is high and at times the VPMs tend to get demagnetized by the adjacent CPMs thus making the operating point of the VPMs very unstable.

2) SERIES HYBRID MEMORY MOTORS

In contrast, in a series hybrid arrangement [6], [32], [33], the CPM flux always flows forward through VPMs as shown in Fig. 6 (b). Hence the CPM flux always assists the VPMs thereby stabilising the operating point of the VPM. Comparative study of the two hybrid models of VFMMs [34] show that the obvious advantage of series hybrid VFMM over parallel design. The complicated rotor flux barriers are avoided in series hybrid VFMM since the VPM working point is inherently stable due to the assistance of CPMs.

Figure 7 shows the B-H curve of the VPM and qualitatively compares the difference in the magnet operating point in a parallel type hybrid rotor and a series type hybrid rotor. The VPM operating points with the parallel type of hybrid connection would be lower than those without CPMs, thus indicating easier demagnetization. In contrast, in a series type hybrid connection, the VPM operating point moves to A_s, C_s, and D_s respectively. If the machine design intends to maintain a fixed VPM flux, CPMs assist the VPMs to withstand unintentional demagnetization caused by armature reaction. Therefore, the machine can handle high armature and high electrical loading. However, this will also lead to difficulty in intentional demagnetization and remagnetization of VPMs.

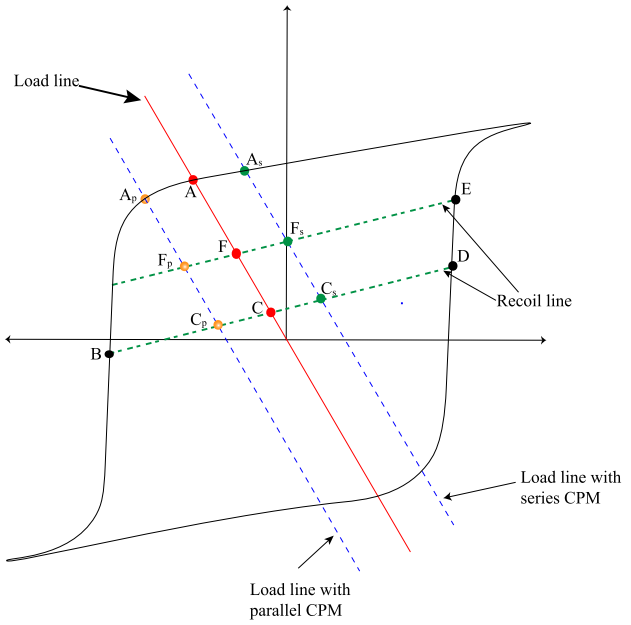

FIGURE 7. Changes in magnet operating point of series and parallel hybrid VFMs [34].

The series type topology can also be found as two variants. That is, either the CPM or VPM can be located on the same rotor pole and connected in series [6], [33] or on alternate rotor poles [32] and connected in series.

Apart from Hybrid Memory motors, one of the alternative state-of-the-art variants of VFMs is the Variable-Flux flux-intensifying motor as reviewed below.

B. VARIABLE-FLUX FLUX-INTENSIFYING INTERIOR PERMANENT MAGNET (VFI-IPM) MACHINES:

In PM Assisted Synchronous Reluctance Machines (PMA-SynRMs) [36], a conventional IPM rotor structure ($L_d < L_q$) is used and a negative d-axis field is imposed together with a q-axis field to produce reluctance torque. If LCF PMs are used, the large magnetic field produced by q-axis currents(i_q) at high load conditions can lower the magnetization levels of the LCF magnets. Both of these fields may cause unintentional demagnetization of the LCF magnets [6], hinder torque production and therefore the magnetization of the LCF magnets will be difficult to control.

In order to effectively utilize reluctance torque in a PMA-SynRM rotor structure while also having controllability of the magnet flux, a significantly modified form of PMA-SynRMs referred to as Variable-Flux Flux-Intensifying Interior Permanent Magnet (VFI-IPM) machines have been studied in the recent past [11]–[15], [17]. The structure of an example 4-pole VFI-IPM machine is shown in Fig. 8 and these type of machines are characteristic in having a positive saliency ($L_d > L_q$). Appropriate design of the IPM rotor with flux barriers to enhance the PM flux with a positive d-axis armature field enables the production of positive reluctance torque with the $L_d > L_q$ characteristics. The positive d-axis armature

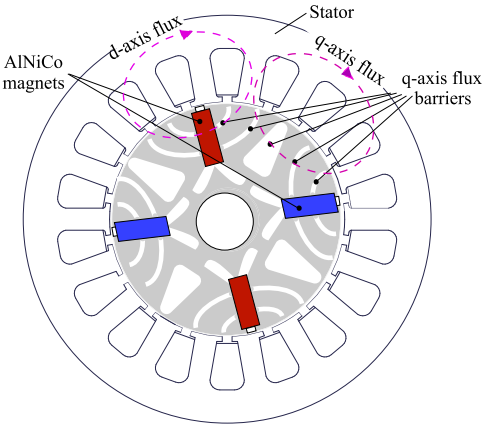

FIGURE 8. Cross section of VFI-IPM motor [14].

field also intensifies the magnetization state thus minimizing the risk of unintentional demagnetization.

Zhu *et al.* [37] show that two 5 kW VFI-IPM motor types achieve a maximum speed of 6900 rpm and 7500 rpm while a conventional machine achieves only 5000 rpm speed. Sun *et al.* [14] demonstrate that with the manipulation of the magnetization of a VFI-IPM machine, the speed is extended from 4000 rpm to 12000 rpm while also maintaining a 94% efficiency in the upper-speed range. Zhu *et al.* of [37] also show that an excessive increase of q-axis flux barriers will lead to saturation of the d-axis flux path, which in turn affects the output torque. Therefore setting an uneven air gap (surface flux barrier) is proposed [37] rather than adding an inner magnetic barrier within the rotor. This ensures better torque output, mechanical robustness, low torque ripple as well as extended speed range. Fukushige *et al.* [13] investigate efficiency characteristics of VFI-IPM for 100%, 75% and 50% Magnetization States (MS) of the magnet. The results show certain benefits of improving efficiency if the MS is maintained at optimal conditions.

III. CHARACTERISTICS OF MAGNETS USED IN VFMS

In conventional PM machines, the PMs have a linear demagnetization region with a superimposed recoil line to ensure stable performance under normal operating conditions. These magnets exhibit high coercivity and are not subjected to irreversible demagnetization under normal operating conditions. Low coercivity magnets such as AlNiCo fail to meet these two expectations and consequently, were superseded by high coercivity magnets such as Samarium Cobalt (SmCo) and Neodymium Iron Boron (NdFeB) for the use in conventional PM motors. However, the aforesaid shortcomings of LCF PMs have been used as a key property in the development of VFM machines. LCF magnets have the following features:

1) A nonlinear demagnetization curve ensures that the recoil line never superimposes on it. Hence, on the removal of demagnetization current, the operating point moves along the recoil line and settles at a lower magnetization level effectively memorizing the magnetization level.

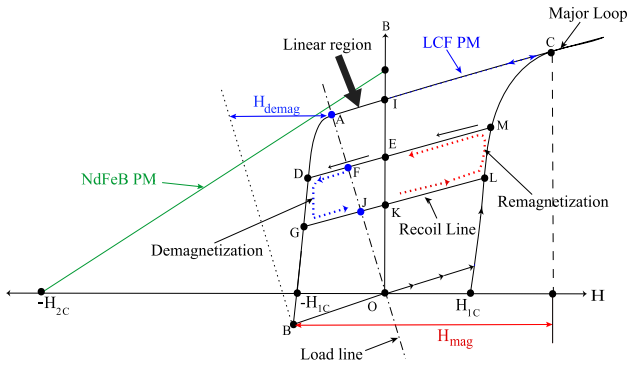

FIGURE 9. Simplified illustration of hysteresis model of LCF PM [34] [35].

2) Low coercivity of magnets makes online demagnetization possible in memory motors. This feature cannot be easily achieved using HCF magnets.

In addition to the above two features, LCF magnets such as AlNiCo exhibit exceptional stability at high temperatures. The unique crystalline bonding between Al, Ni, and Co ensures that the AlNiCo magnets are ideal for high heat applications. Adequately high remanent flux density and a high Curie temperature (approx. 700 to 850°C) is preferable when designing for operation in harsh environments. Therefore, the use of LCF magnets is a good choice for aerospace, automotive and military applications.

A. HYSTERESIS MODEL OF LCF PMS:

PM machines designed to have controllability of the PM flux require an in-depth study of the magnetic material properties. Figure 9 shows the B-H loop for LCF magnets. Point A represents the operating point of the PM at no load conditions. At no load condition, the flux density of the material is lower than its remanent flux density at the point I. This is due to the reluctance of the magnetic circuit. The slope of the load line is known as the Permeance Coefficient (PC).

In the B-H characteristics illustrated in Fig. 9, the PM is fully magnetized at point C and fully demagnetized at point B. If on the application of an external field, the PM operating point moves from point A to point D, the PM will not recoil to point A upon removal of the external field, rather will move to point F. The MS also referred to as Magnetization Level (ML) [38] of a PM is defined as:

$$MS\% = \frac{B_E}{B_I} \times 100\% \tag{1}$$

where B_E and B_I are the magnetic flux densities at points E and I respectively as shown in Fig. 9. The magnetic flux density of point E (B_E) can be calculated as:

$$B_E = B_D - \frac{H_D(B_A - B_I)}{H_A} \tag{2}$$

where B_A, B_I and B_D are the magnetic flux densities at points A, I and D respectively and H_A and H_D are the magnetic field intensities at points A and D.

In order to achieve controllability of PM flux in VFMs, the hysteresis relationship needs to be modeled as closely as possible. The repetitive magnetization/demagnetization behavior of the LCF has been modeled using different approaches such as the Presaich model [19], [39], the Frolich model [40], and piecewise linear models. Yang *et al.* [41] use a Nonlinearity-Involved Parallelogram Hysteresis Model (NIPHM). As shown in Fig. 9, during the Magnetization State change, the LCF magnets undergo a hysteresis process where the operating point traverses the major BH-loop and then recoils along a minor loop. It is typical to assume that the major hysteresis loop and all the minor hysteresis loops have the same value of coercivity however, with different values of remanence.

The intersection of the load line and recoil line determines the operating point of the LCF PM, and the applied MMF determines its displacement on the H axis as shown in Fig. 9. Thus, the PM operating point can be repetitively shifted between different recoil lines by temporarily applying remagnetizing or demagnetizing current pulses. For instance, the operating point of the PM is initiated at F. When applying a demagnetizing current pulse, the operating point will descend to G. After the withdrawal of the current pulse, the operating point will move along a new recoil line and stabilize at new operating point J. On the other hand, when a remagnetizing current pulse is applied, the working point of the PM will track the trajectory of K-L-M-E and return to F.

B. ENERGY STORED AND ENERGY LOSSES IN PM DEMAGNETIZATION/REMAGNETIZTION PROCESS:

The work done on the magnet per unit volume during the magnetization process is given by the total shaded area in Fig. 10 (a). When the external magnetizing force is removed, the orange colored shaded area in Fig. 10 (a) shows the energy stored in the PM. The difference between these two energy changes gives the actual energy dissipated during the cycle of magnetization and demagnetization. This is depicted by the pink colored shaded area in Fig. 10 (a). It is generally dissipated in the form of heat in the magnetic material and is commonly known as the hysteresis loss.

Alternative magnetic materials have also been used for VFMs such as ferrite and lower grades of SmCo as well. The hysteresis curves of these are illustrated below in Fig. 10(b). Ferrite is a good option with its reasonable coercivity (approx. 210 kA/m to 400 kA/m) and a wide linear region, however, the low thermal stability and remanence are the major drawbacks in its implementation. Japanese EV manufacturers [11] have used SmCo magnets due to its more linear hysteresis nature which allows more precise control of flux and magnetization state. Due to high Curie temperature (approx. 720°C), high residual flux density (approx. 0.8 T to 1.0 T) and acceptable coercivity (approx. 160 kA/m to 300 kA/m), SmCo is believed to provide high torque and stable Magnetization States in the cases of heavy loads.

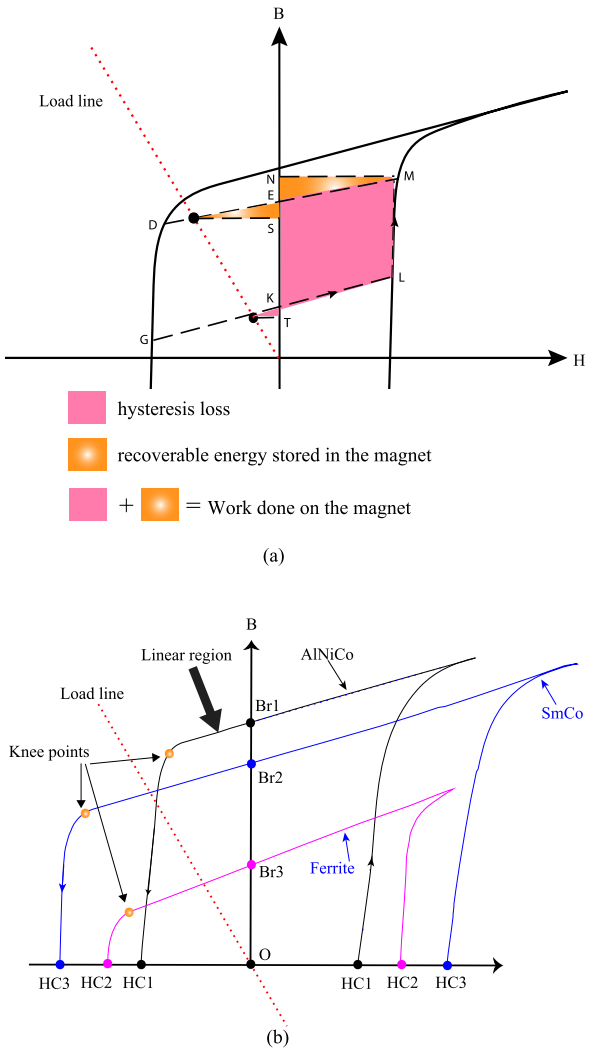

FIGURE 10. **(a) Graphical illustration of work done on magnets and calculation of hysteresis loss [42] and (b) Typical hysteresis curves of LCF magnet material choices [43].**

The ability to manipulate the magnetization of the magnets allows optimization and extension of the operating torque-speed range of VFMs. This is reviewed in detail in the following section.

IV. VFM PRINCIPLE OF OPERATION

VFM operation requires dynamic adjustment of the Magnetization State (MS) primarily as an alternative to field-weakening in traditional PM machine drives. This allows extension of the torque-speed range of the machine. The basic magnetization state manipulation between high speed and low-speed runs of a motor can also be explained using a time-domain illustration as shown in Fig. 11. At low speeds, a positive steady-state current is maintained to achieve optimal torque. As speed increases, it is required to lower the voltage demanded to drive the machine to a high speed. At a speed condition that provides enough voltage margin to control the current, a negative current pulse is imposed to lower the MS. This requires the application of a high voltage, however

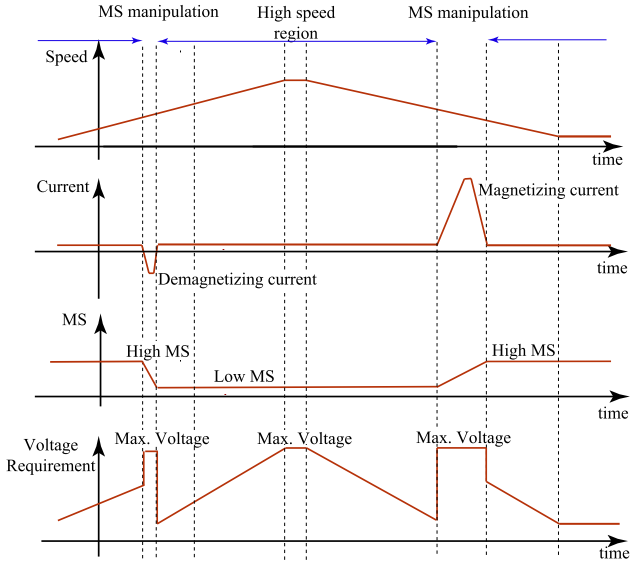

FIGURE 11. **Representative waveforms for MS manipulation with speed and corresponding MS, current and voltage waveforms.**

once applied, the voltage requirement for motor operation is lowered as illustrated in Fig. 11. A weakened PM Field and a lower voltage requirement are achieved for high-speed operation thereby extending the maximum operable speed of the electrical machine. Once the speed transitions from high speed to low speed, a positive current pulse is imposed to enhance the MS to a high state to achieve the high-torque requirements at low speeds.

Further development of the operational principle requires an understanding of the mathematical model of a PM machine. The dynamic model of a PM machine can be written in the d-q synchronous reference frame as [44], [45]:

$$v_d = \frac{d\lambda_d}{dt} + R_s i_d - \omega_e \lambda_q \tag{3}$$

$$v_q = \frac{d\lambda_q}{dt} + R_s i_q + \omega_e \lambda_d \tag{4}$$

where v_d, i_d and v_q, i_q are the d-axis and q-axis voltage and current components. λ_d and λ_q are the d-axis and q-axis flux linkages. R_s is the stator winding resistance and ω_e is the electrical speed of the rotor.

The operation of the machine, is constrained by the maximum inverter voltage and current ($V_{s,\max}$ and $I_{s,\max}$), which can be expressed as:

$$|v_s| = \sqrt{v_d^2 + v_q^2} \leq |V_{s,\max}| \tag{5}$$

$$i_d{}^2 + i_q{}^2 \leq I_{s,\max}^2 \tag{6}$$

If the voltage drop due the resistance is neglected in (3) and (4), (5) can be rewritten in terms of λ_d and λ_q as:

$$\lambda_d^2 + \lambda_q^2 \leq \left(\frac{V_{s,\max}}{\omega_e}\right)^2 \tag{7}$$

The boundaries of (6) and (7) represents circles placed at the origin in i_d-i_q and λ_d-λ_q axes respectively. Yang *et al.* [35]

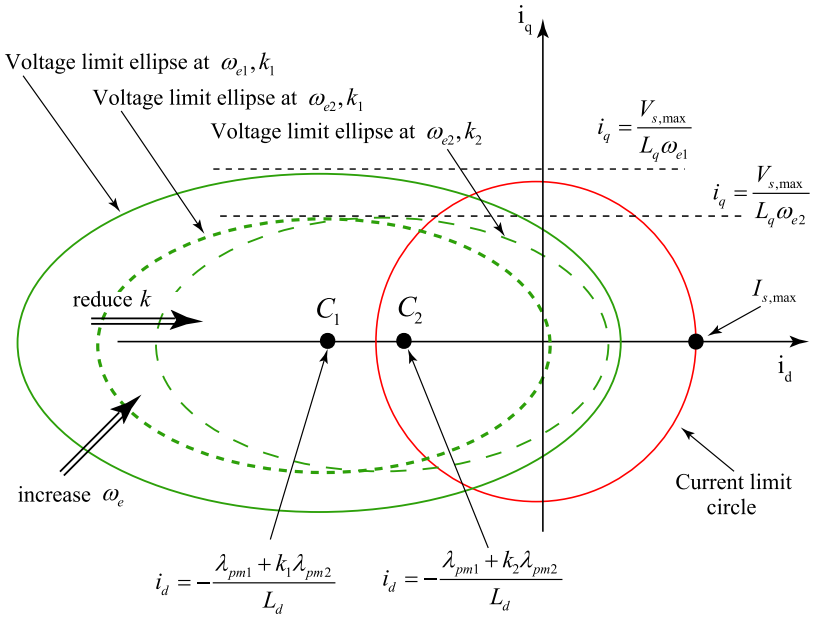

FIGURE 12. Illustration of current limit circle and variation of the voltage limit ellipse with variation of speed and PM flux.

represent the effect of magnetization/remagnetization of the PMs with a variable coefficient k. Then the d-axis and q-axis flux linkages can be represented as:

$$\lambda_d = L_d i_d + \lambda_{pm1} + k\lambda_{pm2} \tag{8}$$

$$\lambda_q = L_q i_q \tag{9}$$

where L_d and L_q are the d-axis and q-axis inductances of the machine. λ_{pm1} and $k\lambda_{pm2}$ represent the flux linkages due the CPMs and VPMs respectively. Variation of $-1 \leq k \leq 1$ represent, the variation of the VPM magnetization from -100% MS to $+100\%$ MS. Substitution of (8) and (9) in (7) yields:

$$\left(i_d + \frac{\lambda_{pm1} + k\lambda_{pm2}}{L_d}\right)^2 + \left(\frac{L_q}{L_d} i_q\right)^2 \leq \left(\frac{V_{s,\max}}{L_d \omega_e}\right)^2 \tag{10}$$

Figure 12 illustrates the shift in the voltage limit ellipse with the variation of speed and with the variation of the magnetization of VPMs. As the machine speed increases, the radius of the voltage limit ellipse decreases as shown in Fig. 12 where $\omega_{e2} < \omega_{e1}$. If the VPM PMs are demagnetized at speed ω_{e2}, this results in a change of the variable k. The center of the voltage circle shifts from C_1 to C_2 as shown in Fig. 12 where $k_2 < k_1$. If the machine has non-salient characteristics, the ellipse tends to a circle as considered in [35].

A. OPERATING MODES OF A VFM:

The operating modes of a VFM have been identified primarily in three torque-speed regions in literature [35], [45]. These include two conventional modes 'constant torque' region and 'field weakening' region as depicted in Fig. 13. However, with VFMs, an additional mode of operation appears within

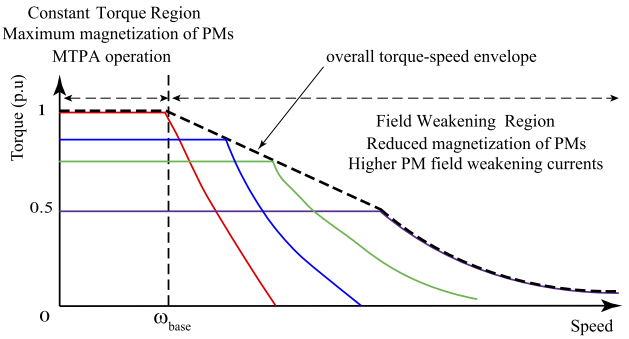

FIGURE 13. Operating regions of VFMs integrating PM magnetization and field weakening control [35]

field weakening mode of operation and can be referred to as the magnetization control mode. The torque developed by a PM machine can be written as:

$$T_e = 3\left(\frac{p}{2}\right)\left\{\left(\lambda_{pm1} + k\lambda_{pm2}\right) i_q + \left(L_d - L_q\right) i_d i_q\right\} \tag{11}$$

In constant torque region, the k is at its maximum and i_d and i_q currents are commanded to achieve optimal operating conditions explained in the following section. In field weakening mode, two parameters exist to control the voltage requirement, namely, parameters k by controlling the magnetization and by controlling the steady-state i_d current as in conventional field weakening. These are further elaborated in the following sections.

1) CONSTANT TORQUE REGION

In constant torque region of operation of PM machines, the torque is mainly limited by the maximum current. In PM machines with significant negative saliency $\left(L_d << L_q\right)$,

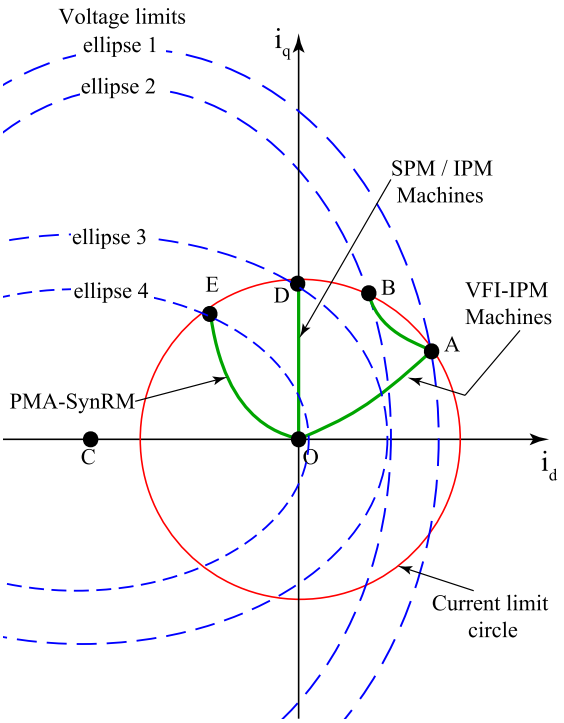

FIGURE 14. Constant torque mode MTPA current trajectory and representation of the base speed operating points C, D and B for PMA-SynRM, IPM or SPM machines and VFI-IPM machines.

such as PMA-SynRMs [36], a maximum torque per ampere (MTPA) strategy can be used to operate the motor in optimal conditions. This would result in $i_d < 0$ and $i_q > 0$ conditions for torque production according to (11). Figure 14 shows the MTPA trajectory O-E for a PM machine with significant negative saliency. The voltage limit ellipse will have a higher radius on the i_d axis compared with the radius on the i_q axis and can be inferred from (10). In PM machines with insignificant saliency $(L_d \approx L_q)$, such as surface PM machines or certain IPM machines, $i_d = 0$ would be optimal and has been considered in [35]. Figure 14 shows the MTPA trajectory O-D for this type of machine.

In contrast, VFI-IPM machines [11] with positive saliency ($L_d >> L_q$), MTPA control would result in $i_d > 0$ and $i_q > 0$. The voltage limit ellipse will have a higher radius on the i_q axis compared with the radius on the i_d axis. The MTPA trajectory O-A represents a low-speed condition. If the speed is increased to a level that the voltage limit ellipse appears prior to the current limit in the trajectory, constant torque can still be maintained under non-optimal conditions with a lower i_d and higher i_q along trajectory A-B as shown in Fig. 14.

Four voltage limit ellipses are shown in Fig. 14. Lower the radius of the voltage limit ellipse, higher the speed. In qualitative terms as shown in Fig. 14, constant torque region can be maintained at high speeds with PMA-SynRM machines than that of SPM machine. However, the constant torque region is limited at a comparatively lower speed in the VFI-IPM machines. The base speeds for the different PM machines are shown by points E, D, and B in Fig. 14. The lower base

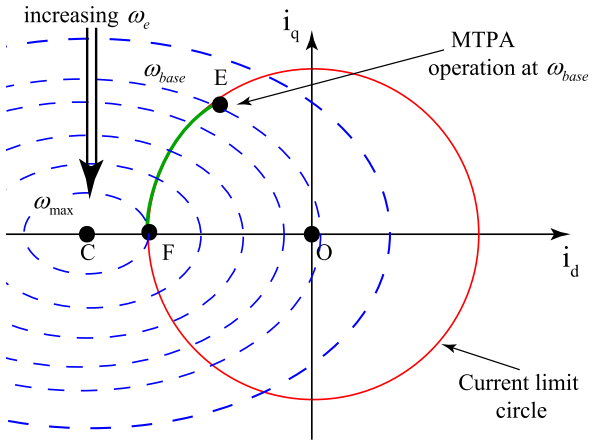

FIGURE 15. Representation of field weakening operation in i_d-i_q plane for conventional PM machines.

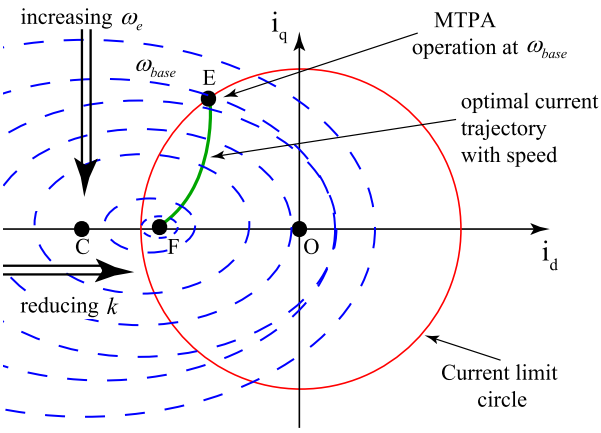

FIGURE 16. Representation of field weakening operation in i_d-i_q plane for negative saliency VFM PM machines.

speed for VFI-IPM machines is due to the positive saliency property. Operation above the base speed for these types of PM machines require Field Weakening (FW).

2) FIELD WEAKENING OPERATION

As explained previously, when speed increases, the radii of the voltage limit ellipse will reduce as depicted in Fig. 15. Beyond the base speed operating point, constant torque cannot be maintained. In conventional PM machines with negative saliency, as the speed increases, i_d is decreased negative to achieve field weakening. The operating point in the i_d-i_q plane will move from E to F along the current limit circle as shown in Fig. 15. The maximum torque production capability will reduce to zero when the current and voltage circles are tangent, i.e., the machine speed reaches the maximum ω_{max}. However, in VFMs the center point C is adjustable by changing the MS, and hence can be shifted towards the origin to achieve an optimal operating point.

Figure 16 shows the increase in speed and the variation of the operating point for a VFM with negative saliency. With an increase in speed, the center of the ellipse can be shifted towards the origin. If the center is located inside the current circle, and the operating speed will not be limited by current

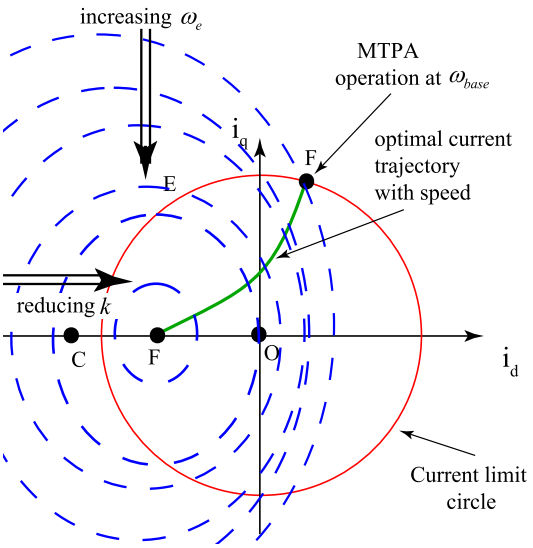

FIGURE 17. Representation of field weakening operation in i_d-i_q plane for positive saliency VFM PM machiness.

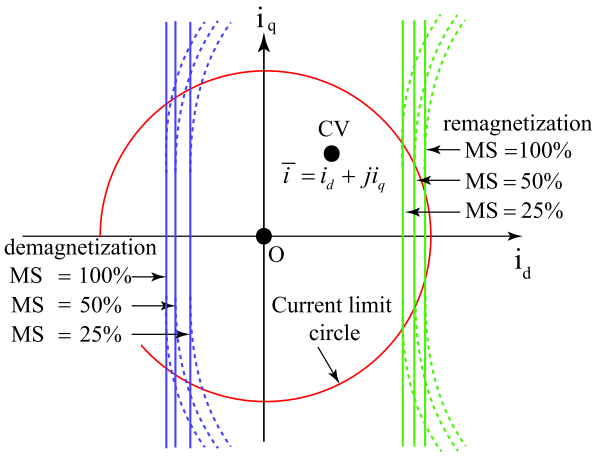

FIGURE 18. i_d boundaries to achieve different MS levels for demagnetization and remagnetizations.

or voltage and therefore theoretically can achieve infinite speed. Figure 16 also depicts the optimal variation of the current and this will be a function of machine parameters. The representation in Fig. 16 is more generic and therefore can be simplified to a vertical line for non-salient PM machines [35].

In [35] MS control is used beyond the base speed to move the center of the voltage limit ellipse towards the origin. After a certain optimal operating point, MS control is disabled and the traditional field weakening is used to extend the speed further.

Figure 17 represent field weakening operation for a VFM with positive saliency. For example, the authors of [45] consider a VFI-IPM motor which has positive saliency and the MS is reduced with speed, and i_d is controlled positive for positive torque production. Although Gagas *et al.* [45] represent a stepwise change in MS, further scope exists to improve control of MS continuously and thus achieve an optimal current trajectory. Theoretically, the machine can achieve infinite speed with field weakening with negative i_d, however, this results in the torque due to the PMs being canceled out by the reluctance torque.

V. MAGNETIZATION STATE MANIPULATION

The adjustment of the MS of VFMs can be achieved in machine design in two different strategies. As explained in the introduction, this is either by designing the machine with dedicated DC magnetization coils or appropriate design of the stator armature winding in AC machines with the ability to produce fields capable of magnetization of the PM material.

A. DC MAGNETIZATION IN VFMS

DC Magnetized Memory Motors need auxiliary DC magnetizing coils to facilitate the magnetization control [35], [46], [47]. By application of a current pulse, a field can be imposed on the magnets to enhance or weaken the magnet flux or even reverse magnetize the magnets.

A hybrid arrangement of magnets may consist of CPMs and VPMs. Yang *et al.* [35] develop a DC-magnetized Switched Flux Memory Motor (SFMM) with a hybrid magnet arrangement. In this type of machine, LCF magnets AlNiCo is used as the VPMs and HCF magnets NdFeB is used as CPMs. The MS of the VPMs can be used to enhance or weaken the overall flux linkage. The 'flux-enhanced' and 'flux-weakened' states refer to $MS = 100\%$ and $MS = -100\%$ respectively. The authors also emphasize the need for coordinated control scheme between the traditional field weakening d-axis current and the magnetization current pulse.

B. AC MAGNETIZED MEMORY MOTORS:

The hysteresis model, and the demagnetization/remagnetization process was explained in Section III. In AC VFMs, the application of demagnetization/remagnetization field is produced by the stator winding and currents. The field that effects the magnetization is primarily the d-axis field and is proportional to the d-axis current.

Fig. 18 shows the i_d boundaries to achieve certain MS levels. For an ideal machine, the q-axis field would not have any effect on the magnetization and therefore the magnetization boundaries would be vertical in the i_d-i_q plane as shown in Fig. 18. However, under practical conditions the q-axis current will also affect the boundary. Gagas *et al.* [45] illustrate the non-ideal magnetization boundaries that are curved at high i_q values as shown by the dotted lines in Fig. 18.

The MS manipulation in VFM machines is achieved by moving the i_d-i_q plane operating point current to the required MS boundary. The i_d-i_q plane operating point is also referred to as the Current Vector (CV): $\bar{i} = i_d + ji_q$. Under normal operation, CV is controlled to produce the desired torque, however, when a change in MS is desired, a short direct axis i_d transient current is applied, after which normal operation is resumed. The application of this i_d transient current moves the CV to the required MS boundary. Thereafter, retraction to the normal operating point will result in recoiling of the

magnetization of the VPMs to the corresponding MS as explain earlier using Fig. 9.

The i_d transient current needs to be coordinated such that the transit torque ripple that arises from the change of MS are mitigated. In addition, the transient current also needs to be imposed such that, once remagnetized the CV does not cross the demagnetization boundary. Different MS manipulation strategies are found in literature [9], [45], [48]–[50]. In general, the i_d and i_q are actively varied as a function of time in all these strategies:

$$i_d = f_{id}(t) \quad and \; i_q = f_{iq}(t) \tag{12}$$

$$\frac{di_d}{dt} = f'_{id}(t) \quad and \; \frac{di_q}{dt} = f'_{iq}(t) \tag{13}$$

Substituting (12) and (13) in (3), (4), (8) and (9) and simplification with neglected resistances yields:

$$v_d = L_d f'_{id}(t) - \omega_e L_q f_{iq}(t) + \lambda_{pm2}\frac{dk}{dt} \tag{14}$$

$$v_q = L_q f'_{iq}(t) + \omega_e L_d f_{id}(t) + \omega_e \lambda_{pm1} + \omega_e k \lambda_{pm2} \tag{15}$$

By appropriate selection of the $f_{id}(t)$ and $f_{iq}(t)$ functions, certain voltage components in (14) and (15) cancel out resulting in the ability to extend the speed at which MS manipulation can be achieved.

1) TRAPEZOIDAL i_d PULSE METHOD:

The use of a trapezoidal i_d current pulse to manipulate the CV is found to be a popular approach due to its simplicity. However this requires higher voltages compared with alternative strategies [9], [42], [48], [50]. Athavale *et al.* [42] compare the trapezoidal approach with an alternative approach referred to as the SLλ^sT approach and is shown to have a longer transient period. If the speed is low, it is possible to maintain constant torque as shown by Yu *et al.* [48]. The speed at which the MS manipulation achievable can be further increased if zero i_q currents are commanded. However, as the trapezoidal i_d pulse method has a long transient period, a zero i_q would impose a significant torque pulse if the machine is running under loaded conditions.

Figure 19 shows the current trajectory for a VFI-IPM machine [48]. The machine is initially at operating point A with $25\% < \text{MS} < 50\%$. The CV is shifted to B to achieve a $\text{MS} = 50\%$. The i_q reduces in this path due to the extra torque produced by the reluctance in the VFI-IPM machine. Once $\text{MS} = 50\%$ is achieved, the CV returns to the MTPA operating point D, which commands a lower i_q due to the higher flux linkage to produce the same torque. If the machine is to be demagnetized, the CV needs to be shifted to the negative i_d region, and Fig. 19 depicts the case where CV moves to point E to achieve a lower MS at 25%. Once the CV returns to the MTPA operating point F, a higher i_q is required to produce the same torque due to the lower PM flux linkage. The magnetization process can also be performed without maintaining constant torque. This is represented by the dotted trajectory AC in Fig. 19 and returning to the MTPA operating point at point D.

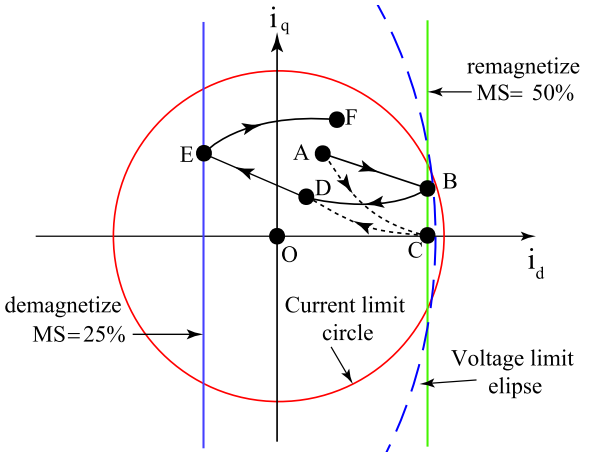

FIGURE 19. CV trajectory under magnetization (AB or AC) and demagnetization (DE) under comparatively low speed conditions - e.g. with trapezoidal i_d pulse method.

Considering the equation (14), the voltage component $\left\{L_d f'_{id}(t) - \omega_e L_q f_{iq}(t)\right\}$ is reduced to zero at Point C due to $i_q = 0$ and the $f'_{id} = 0$. With $f'_{iq}(t) = 0$, the voltage requirement is mainly determined by (15) simplified to:

$$v_q = \omega_e L_d f_{id}(t) + \omega_e \lambda_{pm1} + \omega_e k \lambda_{pm2} \tag{16}$$

Neglecting the effect of $\frac{dk}{dt}$, the speed that limits the remagnetization using the trapezoidal i_d pulse method with a $i_{d,MS\%}$ d-axis current pulse magnitude is given by:

$$\omega_{e,\max} = \frac{V_{s,\max}}{L_d i_{d,MS\%} + \lambda_{pm1} + k\lambda_{pm2}} \tag{17}$$

2) MS STATE MANIPULATION AT HIGH SPEEDS

The trapezoidal current pulse method is suitable for speed conditions where sufficient voltage is available to control the trajectory of the current vector as shown in Fig. 19. However, at high speeds, the available voltage is limited and control of the CV is challenging. At high speeds, MS manipulation simultaneous torque production is not prioritized, rather the mitigation of the torque ripple is considered [45], [49]. Once the VFMs are magnetized, the CV returns to an operating point capable of producing the commanded torque. During this transient, the trajectory may potentially overshoot passing the demagnetization boundary resulting in a lower MS in the VFM. The trajectory shown by the dotted lines in Fig. 20 depicts this condition and as a result, MS manipulation will not be achievable at such speeds.

Two forms of control methods are proposed for MS manipulation at high speeds viz.:

1. Reverse rotating current vector trajectory (RRCVT) MS manipulation [45], [50]

2. Straight Line stationary frame flux linkage Trajectory (SLλ^sT) MS manipulation [9], [42], [50]

- *Reverse rotating current vector trajectory (RRCVT) MS manipulation:*

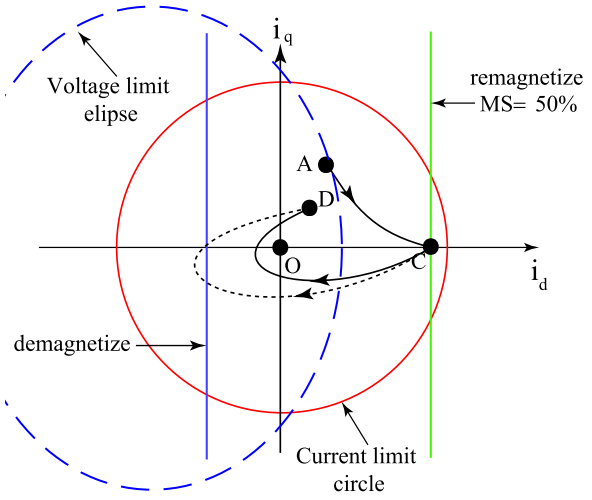

FIGURE 20. CV trajectories at high speeds during remagnetization (AC) and transient returning to steady-state operation (CD) - trajectory dotted line passing the demagnetization boundary / trajectory solid line not passing the demagnetization boundary.

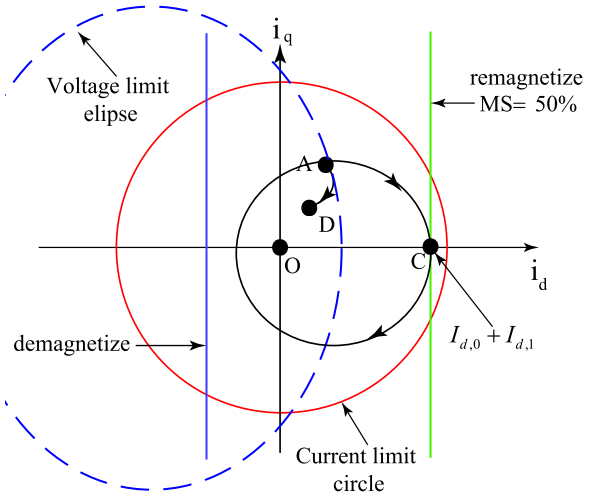

FIGURE 21. CV trajectories during RRCVT magnetization and return to steady-state operating point.

The RRCVT approach uses a sinusoidal variation of the i_d and i_q currents during the MS manipulation period in order to cancel certain voltage dynamics in (14) and (15).

$$f_{id}(t) = I_{d,0} + I_{d,1}\cos(-\omega_e t + \phi) \tag{18}$$
$$f_{iq}(t) = I_{q,0} + I_{q,1}\sin(-\omega_e t + \phi) \tag{19}$$

The derivatives of (18) and (19) are given by:

$$f'_{id}(t) = \omega_e I_{d,1}\sin(-\omega_e t + \phi) \tag{20}$$
$$f'_{iq}(t) = -\omega_e I_{q,1}\cos(-\omega_e t + \phi) \tag{21}$$

Substitution of (18) - (21) in (14) and (15) yields:

$$v_d = L_d\omega_e I_{d,1}\sin(-\omega_e t + \phi) - \omega_e L_q I_{q,0} - \omega_e L_q I_{q,1}\sin(-\omega_e t + \phi) + \lambda_{pm2}\frac{dk}{dt} \tag{22}$$
$$v_q = -L_q\omega_e I_{q,1}\cos(-\omega_e t + \phi) + \omega_e L_d I_{d,0} + \omega_e L_d I_{d,1}\cos(-\omega_e t + \phi) + \omega_e\lambda_{pm1} + \omega_e k\lambda_{pm2} \tag{23}$$

By commanding i_d and i_q such that $L_d I_{d,1} = L_q I_{q,1}$ with $I_{q,0} = 0$ and neglecting the $\frac{dk}{dt}$ term yields:

$$v_d = 0 \tag{24}$$
$$v_q = \omega_e L_d I_{d,0} + \omega_e\lambda_{pm1} + \omega_e k\lambda_{pm2} \tag{25}$$

The speed that limits the remagnetization using the RRCVT method with a $i_{d,MS\%}$ d-axis current pulse magnitude $i_{d,MS\%} = I_{d,0} + I_{d,1}$ is given by:

$$\omega_{e,\max} = \frac{V_{s,\max}}{L_d I_{d,0} + \lambda_{pm1} + k\lambda_{pm2}} \tag{26}$$

By setting appropriate values for $I_{d,0}$ and $I_{d,1}$ in (18), the d-axis current for a certain MS can be achieved. The trajectory of the CV during the MS manipulation stage represents a circle that passes the required MS boundary. By placing the circle appropriately, the demagnetization during the return to steady-state operation can be avoided. Figure 21 shows the trajectory during magnetization without passing the demagnetization boundary. Gagas *et al.* [50] achieve MS manipulation at 146% higher speeds than the Trapezoidal i_d pulse method. By comparison of (17) and (26) it can be seen that since $i_{d,MS\%} > I_{d,0}$, a higher speed can be guaranteed with (26) RRCVT approach.

• *Straight Line stationary frame flux linkage Trajectory (SLλ^sT) MS manipulation:*

In the SLλ^sT approach, the authors employ a very short current pulse compared with the trapezoidal i_d pulse to magnetize the VFMs. This is found to produce a lower torque and speed ripple on the machine due to the short lower pulse period. The SLλ^s technique applies full voltage in the stationary reference frame for a certain period where the flux linkage will increase rapidly. During this period, the corresponding d-axis current crosses the magnetization boundary and thereafter the i_d is lowered by application of a reverse voltage in the stationary reference frame. In contrast to the application of a voltage in the synchronous reference frame, the voltage vector is not rotating in the stationary reference frame and is, therefore, a fixed voltage at the three-phase terminals for the period considered for MS manipulation. Athavale *et al.* [42] identify that the second-half of the SLλ^sT as the main limiting factor at high speeds, where the CV trajectory returning to a steady-state operating condition may lose controllability and pass the demagnetization boundary as shown in Fig. 20.

Gagas *et al.* [45] compare the SLλ^sT approach with the Trapezoidal i_d pulse method and the RRCVT approach. Compared with the Trapezoidal i_d pulse method, the maximum speed at which the MS can be increased to 100% is found to be at 164% higher for the RRCVT approach and 202% higher for the SLλ^sT approach.

VI. MAGNETIZATION STATE ESTIMATION

During VFM operation under dynamic loads and a range of speeds, MS will also be adjusted dynamically. In order to appropriately control the MS, it is necessary to know

the current MS. In a stationary machine, the MS can be measured directly by inserting a magnetometer in the air gap. However, direct measurement of MS is not practical in most of the cases. Alternatively, sensors can be installed beneath the magnets to determine the MS. Such methods require changes in the machine design and additional sensors, cable, and electronics. Therefore, a technique that can provide a reasonably accurate estimation of the MS under loaded and unloaded conditions, and across all torque-speed regimes is preferable.

The MS estimation methods proposed in [45] and [51]–[56] can be classified as High Frequency Injection (HFI) [51] based methods and model-based methods [56].

A. HFI BASED MS ESTIMATION

High-frequency signal injection based methods estimate the PM MS either from the d-axis high-frequency inductance [52] which changes with saturation level or from the PM electrical high-frequency resistance [51], [55], which changes with magnetization state due to magnetoresistive effects. Magnetoresistance (MR), is the change of a material's resistivity with the application of a magnetic field. This method has the advantage of being able to be used over a wide speed range including standstill. MS estimation using the magnetoresistive effect in PMSM using non-segmented NdFeB magnets is discussed in [51]. SmCo and ferrite magnets in addition to NdFeB are analyzed for the magnetoresistive effect in [55] and it has also shown that the estimated high-frequency resistance can be potentially used to distinguish between controlled demagnetization and accidental demagnetization, which is an important feature for fault prognosis. Comparison of the magnetoresistive effect on the different types of magnets indicates that NdFeB shows the highest sensitivity whereas SmCo and ferrites show modest values.

B. MODEL BASED MS ESTIMATION

Model-based methods use Back-EMF estimation to determine PM magnetization states from the stator flux linkage values obtained from the machine terminal voltages and currents, without interfering at all with the normal operation of the machine. Therefore the machine needs to be rotating and hence estimation of MS at standstill is not possible in these methods. In addition, knowledge of machine parameters such as stator resistance, inductance is required to perform an accurate estimation of the MS.

In [53] MS estimation using Neural Networks is proposed. Classical Artificial Neural Networks(ANN) can be used to learn complex physical relations. However, they use a large number of neurons and can be difficult to implement in a controller. Structured Neural Networks (SNNs) take advantage of the known physics to select appropriate network architecture and a combination of physically meaningful basis functions [57]. SNNs can be a useful tool in learning the saturation and cross saturation characteristics of a VFM and represent it in a compact form.

C. SENSITIVITY OF MS ESTIMATION

A number of factors may decrease the accuracy of the MS estimation obtained by a pulsating d-axis high-frequency current. Reigosa *et al.* [58] study the effect of machine assembling tolerances on HFI based temperature estimation of electrical machines, particularly the sensitivity of static eccentricities, dynamic eccentricities, mixed eccentricities, magnet assembling tolerances) and stator/rotor lamination grain orientation. The same issues will also be present with HFI based MS estimation. In addition to assembling tolerances, HFI based methods are sensitive to material properties [52], [55], and operating current, and their bandwidth is limited by the carrier frequency. Also, they require the injection of an additional signal, which can have some adverse effects on the operation of the machine, e.g. extra losses, noise, and vibration.

Further studies by [54] show the contribution of PM coating in enhancing magnetoresistive sensitivity and NdFeB yet again is found to have the highest increment in sensitivity.

VII. PERMANENT MAGNET MATERIALS FOR VARIABLE FLUX MACHINES

SmCo and NdFeB magnets are typically considered in traditional PM machine design due to their high coercivity. These magnets have certain characteristics that enable high power dense machine designs. However, due to the need for rare earth material, significant research has been undertaken for the development of rare-earth-free magnets and/or to reduce the rare-earth content in rare-earth magnets. In review of these techniques, it can be found that some of these newly developed magnetic materials, although they do not achieve comparable properties as SmCo or NdFeB may have certain properties that may be relevant and beneficial to the design of VFMs. The general goal for the development of non-RE PMs is to fill in the gap between the most cost-effective low performing hard ferrite magnets and the expensive high performing RE PMs. This subsection summarises such developments in PM materials technology that are relevant for VFM design.

A. EMPLOYING NON-CRITICAL RARE-EARTH MATERIALS SUCH AS CERIUM FOR DOPING OF NDFEB

Doping of NdFeB magnets with RE material such as Cerium (Ce), Lanthanum (La) and Praseodymium (Pr) have been investigated in the past. For example, Kim *et al.* [59] investigate different ratios of multiple RE Trifluorides with NeFeB melt-spun flakes. The coercive force (Hci) that represent the magnet's resistance to demagnetization is found to substantially deteriorate in order: DyF_3, NdF_3, PrF_3, LaF_3 and lowest with CeF_3. Chen *et al.* [60], Das *et al.* present the properties of magnets with Ce or Pr instead of Nd. In contrast, Chen *et al.* [60] have recently studied the mixture of Nd, Pr and Ce and properties of such magnets and it has been shown that addition of Ce lowers the coercivity of magnets significantly. Therefore, the substitution of non-critical RE material in magnets appear to be an alternative approach to manufacture LCF magnetic material suitable for VFMs.

B. RARE-EARTH FREE PERMANENT MAGNETIC MATERIALS SUCH AS MNBI

MnBi intermetallic compounds have shown different magnetic characteristics than other magnetic material. The theoretical maximum energy product of MnBi is found to be 127 kJ/m^3 [62] and is also found to have coercivity suitable for VFMs. In addition, MnBi positive temperature coefficient of coercive force is beneficial for VFM designs to operate in high-temperature environments. The coercivity mechanism of MnBi alloys is strongly dependent on phase constitution and microstructural features. When MnBi magnets are manufactured in hard phase to be exchange-coupled with a soft phase, the remanent magnetization can be improved to >10 kG while coercivity is maintained at >800 kA/m. By adapting the manufacturing technique, it is, therefore, possible to manufacture MnBi magnets suitable for VFMs not necessarily with high coercivity.

C. DEVELOPMENT OF NANOSTRUCTURED MAGNETIC MATERIALS

Recent advancements in nanotechnology have achieved certain materials with properties that exhibit magnetism in nano-scale. By appropriate manufacturing techniques, it is possible to refine the magnetic properties of the material to suit VFMs. Manufacturing techniques such as melt spinning, gas-aggregation-type cluster-deposition, and thin-film processing methods produce nanostructured rare-earth-free materials that may exhibit LCF properties. Some investigations on nanostructured rare-earth-free magnetic material are based on Co-rich transition-metal alloys ($HfCo_7$ and Zr_2Co_{11}) [61], [63], Manganese based compounds [62], [64], cobalt-ferrite nanoparticles [65], and FePt-based nanocomposites [66]. However, the high cost of Pt and Hf elements is a prohibitive factor for mass production of certain nanostructured rare-earth-free permanent magnetic material and require further research and development.

D. MODIFICATION OF MAGNETIC MATERIALS DEVELOPED PRE NDFEB MAGNET ERA

Lanthanum based ferrite magnets [64] have been used prior to NdFeB technology. However, such magnets exhibit properties beneficial for VFM design. Lanthanum is also rare-earth material, however, it is cheaper than Neodymium and therefore has the potential to be used as magnetic materials for VFM design.

E. MODIFICATION OF NDFEB MAGNET MANUFACTURING TECHNIQUES

The coercive force of pure NdFeB is not high enough for application in conventional fixed flux electric machines. These magnets are therefore mixed with Dysprosium (Dy) to improve the coercive force and high-temperature performance. The possibility to alter the use of Dy or use of an alternative compound in NdFeB magnet manufacture offers the possibility to create LCF magnets that may offer advantageous characteristics for VFM design. For example,

TABLE 2. Performance comparison of two IPM motors with different magnets [67].

	Unit	N35EH	New Magnet
H_c of magnets(150°C)	kA/m	744	446
B_r of magnets(150°C)	T	1.00	1.20
Efficiency at rated point	%	93.22	94.26
Efficiency at peak point	%	86.63	89.27
Efficiency over NEDC	%	93.84	93.41
Efficiency over Artemis	%	92.78	93.67

Chen *et al.* [67] present a manufacturing technique for $Nd_2Fe_{14}B$ magnets by Grain Boundary Diffusion Processing (GBDP). The magnet properties are summarized in Table 2. It is shown that the GBDP reduces the required Dy material by 81%, while also increasing the Br by 17%. The H_{cj} value is between that of grades of N35EH and N38H. The ability to control the H_{cj} using the GBD process in NdFeB permanent magnet can be considered as one of the technologies that could lead to a new class of magnets suitable for VFMs.

VIII. CONCLUSION AND DISCUSSIONS

This paper has reviewed the variable-flux machine (VFM) concept and has compared different VFM topologies, modeling and control strategies, and materials. The VFM topologies, mainly the parallel hybrid PM type, the series hybrid PM type and Variable-Flux Flux Intensifying type VFMs are discussed in detail. It is found that the VFI-IPM machines offer superior characteristics for VFM operation due to armature currents intensifying the magnetization of the PMs thus minimizing the risk of unintentional demagnetization. To achieve wide speed in VFMs, the LCF PMs have to be used owing to its nonlinear demagnetization characteristics in the second quadrant of the B-H curve. The process of magnetization, demagnetization and energy loss during this process has been explained using the B-H characteristics of the magnet material. The general VFM characteristics and the concept of 'magnetization state' have been presented. The magnetization/demagnetization analysis of major types of VFM topologies have also been discussed. The various MS manipulation schemes depending on the various topologies of VFMs are reviewed in detail and limiting factors are identified. MS estimation techniques of various VFM topologies are reviewed and summarized. The development of rare-earth-free permanent-magnet alloys and potential alternative magnetic material that can satisfy the requirements of VFMs have been identified. From the review, following challenges and future trends in VFM technology have been identified:

1) VFMs with features such as improved torque density, extended torque-speed range, magnetization state manipulation capability at high speeds, lower magnetizing current requirements and reduced risk of unintentional demagnetization are highly desirable.
2) Accurate MS estimation strategies remain underdeveloped and can improve and complement the dynamic performance of VFMs.
3) Non-RE PMs do not exhibit high magnetization and high coercivity simultaneously. High coercivity can be achieved by either the materials intrinsic high

magnetocrystalline anisotropy, fine particle/grain size, or shape anisotropy. Therefore, VFMs can benefit from hybridization with the use of multiple magnetic material types in the design of the rotor.

4) Further development in electromagnetic tools for VFMs remains to be developed. A mathematical model of the hysteresis with magnetization/demagnetization process of LCF magnets is not popularly available to-date. Development of such tools will provide means to further optimization of VFMs by future researchers.

REFERENCES

[1] L. Xu, L. Ye, L. Zhen, and A. El-Antably, "A new design concept of permanent magnet machine for flux weakening operation," *IEEE Trans. Ind. Appl.*, vol. 31, no. 2, pp. 373–378, Mar. 1995.

[2] T. A. Lipo and M. Aydin, "Field weakening of permanent magnet machines–design approaches," in *Proc. EPE Power Electron. Motion Control Conf. (EPE-PEMC)*, 2004, pp. 1–7.

[3] M. Tursini, E. Chiricozzi, and R. Petrella, "Feedforward flux-weakening control of surface-mounted permanent-magnet synchronous motors accounting for resistive voltage drop," *IEEE Trans. Ind. Electron.*, vol. 57, no. 1, pp. 440–448, Jan. 2010.

[4] M. Humphries, *Rare Earth Elements: The Global Supply Chain*. Washington, DC, USA: Congressional Research Service Technical Report, 2011.

[5] Z. Q. Zhu and D. Howe, "Electrical machines and drives for electric, hybrid, and fuel cell vehicles," *Proc. IEEE*, vol. 95, no. 4, pp. 746–765, Apr. 2007.

[6] K. Sakai, K. Yuki, Y. Hashiba, N. Takahashi, and K. Yasui, "Principle of the variable-magnetic-force memory motor," in *Proc. Int. Conf. Elect. Mach. Syst.*, Nov. 2009, pp. 1–6.

[7] V. Ostovic, "Memory motors-a new class of controllable flux PM machines for a true wide speed operation," in *Proc. 36th IEEE Ind. Appl. Conf. Rec. IAS Annu. Meeting*, vol. 4, Sep./Oct. 2001, pp. 2577–2584.

[8] V. Ostovic, "Memory motors," *IEEE Ind. Appl. Mag.*, vol. 9, no. 1, pp. 52–61, Jan. 2003.

[9] S. Maekawa, K. Yuki, M. Matsushita, I. Nitta, Y. Hasegawa, T. Shiga, T. Hosoito, K. Nagai, and H. Kubota, "Study of the magnetization method suitable for fractional-slot concentrated-winding variable magnetomotive-force memory motor," *IEEE Trans. Power Electron.*, vol. 29, no. 9, pp. 4877–4887, Sep. 2014.

[10] C. C. Pavel, C. Thiel, S. Degreif, D. Blagoeva, M. Buchert, D. Schüler, and E. Tzimas, "Role of substitution in mitigating the supply pressure of rare earths in electric road transport applications," *Sustain. Mater. Technol.*, vol. 12, pp. 62–72, Jul. 2017.

[11] N. Limsuwan, T. Kato, K. Akatsu, and R. D. Lorenz, "Design and evaluation of a variable-flux flux-intensifying interior permanent magnet machine," in *Proc. IEEE Energy Convers. Congr. Expo. (ECCE)*, Sep. 2012, pp. 3670–3677.

[12] T. Kato, N. Limsuwan, C.-Y. Yu, K. Akatsu, and R. D. Lorenz, "Rare earth reduction using a novel variable magnetomotive force flux-intensified IPM machine," *IEEE Trans. Ind. Appl.*, vol. 50, no. 3, pp. 1748–1756, May/Jun. 2014.

[13] T. Fukushige, N. Limsuwan, T. Kato, K. Akatsu, and R. D. Lorenz, "Efficiency contours and loss minimization over a driving cycle of a variable-flux flux-intensifying interior permanent magnet machine," in *Proc. IEEE Energy Convers. Congr. Expo.*, Sep. 2013, pp. 591–597.

[14] A. Sun, J. Li, R. Qu, B. Zhao, D. Li, H. Fang, and Y. Sun, "Magnetization and performance analysis of a variable-flux flux-intensifying interior permanent magnet machine," in *Proc. IEEE Int. Electr. Mach. Drives Conf. (IEMDC)*, May 2015, pp. 369–375.

[15] A. Sun, J. Li, R. Qu, J. Chen, and H. Lu, "Rotor design considerations for a variable-flux flux-intensifying interior permanent magnet machine with improved torque quality and reduced magnetization current," in *Proc. IEEE Energy Convers. Congr. Expo. (ECCE)*, Sep. 2015, pp. 784–790.

[16] Y. Lu, J. Li, R. Qu, and A. Sun, "Design and analysis of a hybrid permanent magnet variable-flux flux-intensifying machine," in *Proc. 19th Int. Conf. Elect. Mach. Syst. (ICEMS)*, Nov. 2016, pp. 1–6.

[17] N. Limsuwan, T. Fukushige, K. Akatsu, and R. D. Lorenz, "Design methodology for variable-flux, flux-intensifying interior permanent magnet machines for an electric-vehicle-class inverter rating," in *Proc. IEEE Energy Convers. Congr. Expo.*, Sep. 2013, pp. 1547–1554.

[18] I. Boldea, L. N. Tutelea, L. Parsa, and D. Dorrell, "Automotive electric propulsion systems with reduced or no permanent magnets: An overview," *IEEE Trans. Ind. Electron.*, vol. 61, no. 10, pp. 5696–5711, Oct. 2014.

[19] H. B. Lim, Y. H. Kim, M. M. Lee, J. H. Lee, and J. S. Chun, "Permanent magnet demagnetization characteristics analysis of a variable flux memory motor using coupled Preisach modeling and FEM," in *Proc. IEEE Int. Electr. Mach. Drives Conf.*, vol. 1, May 2007, pp. 647–651.

[20] Y. H. Kim and J. H. Lee, "Magnetization phenomenon for variable flux memory motor using finite element method and experimental verification," *J. Magn.*, vol. 21, no. 4, pp. 629–634, 2016.

[21] H. Liu, H. Lin, S. Fang, and Z. Q. Zhu, "Permanent magnet demagnetization physics of a variable flux memory motor," *IEEE Trans. Magn.*, vol. 45, no. 10, pp. 4736–4739, Oct. 2009.

[22] H. Liu, H. Lin, Z. Q. Zhu, M. Huang, and P. Jin, "Permanent magnet remagnetizing physics of a variable flux memory motor," *IEEE Trans. Magn.*, vol. 46, no. 6, pp. 1679–1682, Jun. 2010.

[23] A. Takbash and P. Pillay, "Magnet design consideration of a variable-flux PM machine," in *Proc. IEEE Energy Convers. Congr. Expo. (ECCE)*, Oct. 2017, pp. 3935–3941.

[24] L. Hengchuan, L. Heyun, F. Shuhua, and H. Xueliang, "Investigation of influence of permanent magnet shape on field-control parameters of variable flux memory motor with FEM," in *Proc. World Automat. Congr.*, Sep./Oct. 2008, pp. 1–4.

[25] M. Ibrahim, L. Masisi, and P. Pillay, "Design of variable flux permanent-magnet machine for reduced inverter rating," *IEEE Trans. Ind. Appl.*, vol. 51, no. 5, pp. 3666–3674, Sep./Oct. 2015.

[26] M. Ibrahim and P. Pillay, "Design of high torque density variable flux permanent magnet machine using alnico magnets," in *Proc. IEEE Energy Convers. Congr. Expo. (ECCE)*, Sep. 2014, pp. 3535–3540.

[27] H. Yang, H. Lin, Z. Q. Zhu, and S. Lyu, "Novel variable reluctance hybrid magnet memory machines," in *Proc. 20th Int. Conf. Elect. Mach. Syst. (ICEMS)*, Aug. 2017, pp. 1–6.

[28] D. Wu, X. Liu, Z. Q. Zhu, A. Pride, R. Deodhar, and T. Sasaki, "Novel switched flux hybrid magnet memory motor," in *Proc. 7th IET Int. Conf. Power Electron., Mach. Drives (PEMD)*, Apr. 2014, pp. 1–6.

[29] Y. Chen, W. Pan, Y. Wang, R. Tang, and J. Wang, "Interior composite-rotor controllable-flux PMSM-memory motor," in *Proc. Int. Conf. Elect. Mach. Syst.*, vol. 1, Sep. 2005, pp. 446–449.

[30] Y. Zhou, Y. Chen, and J.-X. Shen, "Analysis and improvement of a hybrid permanent-magnet memory motor," *IEEE Trans. Energy Convers.*, vol. 31, no. 3, pp. 915–923, Sep. 2016.

[31] D. Wu, Z. Q. Zhu, X. Liu, A. Pride, R. Deodhar, and T. Sasaki, "Cross coupling effect in hybrid magnet memory motor," in *Proc. 7th IET Int. Conf. Power Electron., Mach. Drives (PEMD)*, Apr. 2014, pp. 1–6.

[32] H. Hua, Z. Q. Zhu, A. Pride, R. Deodhar, and T. Sasaki, "A novel variable flux memory machine with series hybrid magnets," *IEEE Trans. Ind. Appl.*, vol. 53, no. 5, pp. 4396–4405, Sep./Oct. 2017.

[33] A. Athavale, K. Sasaki, B. S. Gagas, T. Kato, and R. D. Lorenz, "Variable flux permanent magnet synchronous machine (VF-PMSM) design methodologies to meet electric vehicle traction requirements with reduced losses," *IEEE Trans. Ind. Appl.*, vol. 53, no. 5, pp. 4318–4326, Sep./Oct. 2017.

[34] H. Hua, Z. Q. Zhu, A. Pride, R. Deodhar, and T. Sasaki, "Comparative study of variable flux memory machines with parallel and series hybrid magnets," in *Proc. IEEE Energy Convers. Congr. Expo. (ECCE)*, Oct. 2017, pp. 3942–3949.

[35] H. Yang, S. Lyu, H. Lin, Z. Q. Zhu, F. Peng, E. Zhuang, S. Fang, and Y. Huang, "Stepwise magnetization control strategy for DC-magnetized memory machine," *IEEE Trans. Ind. Electron.*, vol. 66, no. 6, pp. 4273–4285, Jun. 2019.

[36] D.-K. Ngo, M.-F. Hsieh, and T. A. Huynh, "Torque enhancement for a novel flux intensifying PMa-SynRM using surface-inset permanent magnet," *IEEE Trans. Magn.*, to be published.

[37] X. Zhu, W. Wu, S. Yang, Z. Xiang, and L. Quan, "Comparative design and analysis of new type of flux-intensifying interior permanent magnet motors with differentq-axis rotor flux barriers," *IEEE Trans. Energy Convers.*, vol. 33, no. 4, pp. 2260–2269, Dec. 2018.

[38] A. Takbash and P. Pillay, "Magnetization and demagnetization energy estimation and torque characterization of a variable-flux machine," *IEEE Trans. Energy Convers.*, vol. 33, no. 4, pp. 1837–1845, Dec. 2018.

[39] S. Y. R. Hui and J. Zhu, "Numerical modelling and simulation of hysteresis effects in magnetic cores using transmission-line modelling and the Preisach theory," *IEE Proc.-Electr. Power Appl.*, vol. 142, no. 1, pp. 57–62, Jan. 1995.

[40] H. Yang, H. Lin, S. Fang, Z. Q. Zhu, and Y. Huang, "Flux-regulatable characteristics analysis of a novel switched-flux surface-mounted PM memory machine," *IEEE Trans. Magn.*, vol. 50, no. 11, pp. 1–4, Nov. 2014.
[41] H. Yang, H. Lin, J. Dong, J. Yan, Y. Huang, and S. Fang, "Analysis of a novel switched-flux memory motor employing a time-divisional magnetization strategy," *IEEE Trans. Magn.*, vol. 50, no. 2, pp. 849–852, Feb. 2014.
[42] A. Athavale, B. S. Gagas, R. D. Lorenz, K. Sasaki, and T. Kato, "Effect of dynamic magnetization manipulation on transient losses and magnet temperature in energy-saving VF-PMSM traction drives," in *Proc. 19th Eur. Conf. Power Electron. Appl. (EPE ECCE Eur.)*, Sep. 2017, pp. P.1–P.10.
[43] H. Yang, Z. Q. Zhu, H. Lin, P. L. Xu, H. L. Zhan, S. Fang, and Y. Huang, "Design synthesis of switched flux hybrid-permanent magnet memory machines," *IEEE Trans. Energy Convers.*, vol. 32, no. 1, pp. 65–79, Mar. 2017.
[44] P. C. Krause, O. Wasynczuk, and S. D. Sudhoff, *Analysis of Electric Machinery and Drive Systems*. Piscataway, NJ, USA: IEEE Press, 2002.
[45] B. S. Gagas, K. Sasaki, T. Fukushige, A. Athavale, T. Kato, and R. D. Lorenz, "Analysis of magnetizing trajectories for variable flux PM synchronous machines considering voltage, high-speed capability, torque ripple, and time duration," *IEEE Trans. Ind. Appl.*, vol. 52, no. 5, pp. 4029–4038, Sep./Oct. 2016.
[46] C. Yu and K. T. Chau, "Design, analysis, and control of DC-excited memory motors," *IEEE Trans. Energy Convers.*, vol. 26, no. 2, pp. 479–489, Jun. 2011.
[47] C. Yu and K. T. Chau, "Dual-mode operation of DC-excited memory motors under flux regulation," *IEEE Trans. Ind. Appl.*, vol. 47, no. 5, pp. 2031–2041, Sep./Oct. 2011.
[48] C.-Y. Yu, T. Fukushige, N. Limsuwan, T. Kato, D. D. Reigosa, and R. D. Lorenz, "Variable-flux machine torque estimation and pulsating torque mitigation during magnetization state manipulation," in *Proc. IEEE Energy Convers. Congr. Expo.*, Sep. 2013, pp. 852–859.
[49] B. S. Gagas, K. Sasaki, A. Athavale, T. Kato, and R. D. Lorenz, "Magnet temperature effects on the useful properties of variable flux PM synchronous machines and a mitigating method for magnetization changes," *IEEE Trans. Ind. Appl.*, vol. 53, no. 3, pp. 2189–2199, May/Jun. 2017.
[50] B. Gagas, T. Fukushige, T. Kato, and R. D. Lorenz, "Operating within dynamic voltage limits during magnetization state increases in variable flux PM synchronous machines," in *Proc. IEEE Energy Convers. Congr. Expo. (ECCE)*, Sep. 2014, pp. 5206–5213.
[51] D. Reigosa, D. Fernandez, Z.-Q. Zhu, and F. Briz, "PMSM magnetization state estimation based on stator-reflected PM resistance using high-frequency signal injection," *IEEE Trans. Ind. Appl.*, vol. 51, no. 5, pp. 3800–3810, Sep./Oct. 2015.
[52] C.-Y. Yu, T. Fukushige, A. Athavale, B. Gagas, K. Akatsu, D. Reigosa, and R. D. Lorenz, "Zero/low speed magnet magnetization state estimation using high frequency injection for a fractional slot variable flux-intensifying interior permanent magnet synchronous machine," in *Proc. IEEE Energy Convers. Congr. Expo. (ECCE)*, Sep. 2014, pp. 2495–2502.
[53] A. Athavale, K. Sasaki, T. Kato, and R. D. Lorenz, "Magnetization state estimation in variable-flux PMSMs," in *Proc. IEEE Int. Electr. Mach. Drives Conf. (IEMDC)*, May 2017, pp. 1–8.
[54] D. Fernandez, D. Reigosa, J. M. Guerrero, Z. Q. Zhu, C. Suarez, and F. Briz, "Influence of PM coating on PM magnetization state estimation methods based on magnetoresistive effect," *IEEE Trans. Ind. Appl.*, vol. 54, no. 3, pp. 2141–2150, May/Jun. 2018.
[55] D. Fernandez, D. Reigosa, J. M. Guerrero, Z.-Q. Zhu, and F. Briz, "Permanent magnet magnetization state estimation using high frequency signal injection," in *Proc. IEEE Energy Convers. Congr. Expo. (ECCE)*, Sep. 2015, pp. 3949–3956.
[56] H. Min-Fu, D. G. Dorrell, L. Ching-Kuo, C. Po-Ting, and P. Y. P. Wung, "Modeling and effects of *in situ* magnetization of isotropic ferrite magnet motors," *IEEE Trans. Ind. Appl.*, vol. 50, no. 1, pp. 364–374, Jan./Feb. 2014.
[57] P. Garcia, F. Briz, D. Raca, and R. D. Lorenz, "Saliency-tracking-based sensorless control of AC machines using structured neural networks," *IEEE Trans. Ind. Appl.*, vol. 43, no. 1, pp. 77–86, Jan. 2007.
[58] D. Reigosa, D. Fernandez, T. Tanimoto, T. Kato, and F. Briz, "Sensitivity analysis of high frequency signal injection based temperature estimation methods to machine, assembling tolerances," in *Proc. IEEE Energy Convers. Congr. Expo. (ECCE)*, Sep. 2015, pp. 6122–6129.
[59] J. Y. Kim, H.-W. Kwon, J. G. Lee, and J. H. Yu, "Effect of rare-earth dopant on coercivity of hot-pressed Nd–Fe–B magnet doped with RF_3," *IEEE Trans. Magn.*, vol. 51, no. 11, Nov. 2015, Art. no. 2104404.
[60] Z. Chen, Y. K. Lim, and D. Brown, "Substitution of Ce for (Nd,Pr) in melt-spun (Nd,Pr)–Fe–B Powders," *IEEE Trans. Magn.*, vol. 51, no. 11, Nov. 2015, Art. no. 2102104.
[61] B. Das, B. Balamurugan, P. Kumar, R. Skomski, V. R. Shah, J. E. Shield, A. Kashyap, and D. J. Sellmyer, "$HfCo_7$-based rare-earth-free permanent-magnet alloys," *IEEE Trans. Magn.*, vol. 49, no. 7, pp. 3330–3333, Jul. 2013.
[62] K. W. Moon, K.-W. Jeon, M. Kang, M.-K. Kang, Y. Byun, J. B. Kim, H. Kim, and J. Kim, "Synthesis and magnetic properties of MnBi(LTP) magnets with high-energy product," *IEEE Trans. Magn.*, vol. 50, no. 11, Nov. 2014, Art. no. 2103804.
[63] B. Balasubramanian, B. Das, R. Skomski, W. Y. Zhang, and D. J. Sellmyer, "Novel nanostructured rare-earth-free magnetic materials with high energy products," *Adv. Mater.*, vol. 25, no. 42, pp. 6090–6093, 2013.
[64] J. M. D. Coey, "New permanent magnets; manganese compounds," *J. Phys., Condens. Matter*, vol. 26, Jan. 2014, Art. no. 064211.
[65] A. López-Ortega, E. Lottini, C. de J. Fernández, and C. Sangregorio, "Exploring the magnetic properties of ferrite nanoparticles for the development of rare-earth-free permanent magnet," in *Proc. Int. Conf. Comput. Tool (EUROCON)*, Sep. 2015, p. 1.
[66] D. J. Sellmyer, B. Balamurugan, W. Y. Zhang, B. Das, R. Skomski, P. Kharel, and Y. Liu "Advances in rare-earth-free permanent magnets, " in *Proc. 8th Pacific Rim Int. Congr. Adv. Mater. Process.*, F. Marquis, ed. Cham, Switzerland: Springer, 2016, pp. 1689–1696.
[67] L. Chen, D. Hopkinson, J. Wang, A. Cockburn, M. Sparkes, and W. O. Neill, "Reduced dysprosium permanent magnets and their applications in electric vehicle traction motors," *IEEE Trans. Magn.*, vol. 51, no. 11, pp. 1–4, Nov. 2015.

REKHA JAYARAJAN received the B.Tech. degree in electrical and electronics engineering from the University of Calicut, India, in 2008, the B.S. degree from Abdur Rahman University, Chennai, India, and the M.Tech. degree in power electronics from the National Institute of Technology, Calicut, in 2010. She is currently pursuing the Ph.D. degree with RMIT University, Melbourne, Australia. She has served as a Research Assistant with the Indian Space Research Organisation (ISRO) and has held academic positions with the National Institute of Technology, Calicut. Her research interest includes permanent magnet machine design and specifically on variable flux PM machines.

NUWANTHA FERNANDO (M'10) received the B.Sc. degree in electrical engineering from the University of Moratuwa, Sri Lanka, in 2008, and the Ph.D. degree from The University of Manchester, U.K., in 2012. He has been a Researcher with the University of Nottingham and also with University of Oxford. He is currently a Lecturer with RMIT University, Melbourne. His research interest includes electric machines and drives, particularly for electric transportation applications. He serves as an Editor for the IEEE TRANSACTIONS ON ENERGY CONVERSION.

INAM ULLAH NUTKANI (SM'14) received the B.E. degree in electrical engineering from the NED University of Engineering and Technology, Karachi, Pakistan, in 2003, and the M.S. and Ph.D. degrees in electrical power engineering from Nanyang Technological University, Singapore, in 2007 and 2014, respectively. He has been working in different domains of power system with power utilities, regulators, industry, and research organizations, including K-Electric, Karachi, NESCOM, Islamabad, West Energy, Singapore, JM Pang & Seah Singapore and Experimental Power Grid Centre (EPGC), A*STAR, Singapore, from 2003 to 2016. He is currently a Lecturer with the School of Engineering, RMIT University, Melbourne, Australia. His research interests include renewable, distributed generation and microgrids, power electronics and control, and next generation electricity grids.